Electronic Supplementary Material (ESI) for Catalysis Science & Technology.
This journal is © The Royal Society of Chemistry 2022

Supporting Information

Covalent Triazine Frameworks with Cobalt-Loading for Visible Light-Driven Photocatalytic Water Oxidation

Hongmei Chen,[a] Adrian M. Gardner,[b] Guoan Lin,[c] Wei Zhao,[a] Mounib Bahri,[d] Nigel D. Browning,[d] Reiner Sebastian Sprick [a,e] Xiaobo Li[f,a,] Xiaoxiang Xu[c,*] and Andrew I. Cooper[a,*]*

[a]Department of Chemistry and Materials Innovation Factory, University of Liverpool, Liverpool L7 3NY, U.K.
[b]Stephenson Institute for Renewable Energy, University of Liverpool, Liverpool L69 7ZF, U.K.
[c]Clinical and Central Lab, Putuo People's Hospital and Shanghai Key Lab of Chemical, Assessment and Sustainability, School of Chemical Science and Engineering, Tongji University, Shanghai 200060, China
[d]Albert Crewe Centre for Electron Microscopy, University of Liverpool, Liverpool L69 3GL, U.K.
[e]Department of Pure and Applied Chemistry, University of Strathclyde, Thomas Graham Building, 295 Cathedral Street, Glasgow G1 1XL, U.K.
[f]Key Laboratory of the Ministry of Education for Advanced Catalysis Materials, Zhejiang Key Laboratory for Reactive Chemistry on Solid Surfaces, Institute of Physical Chemistry, Zhejiang Normal University, Jinhua 321004, China

Monomer synthesis

Terephthalamidine dihydrochloride [1]: Benzene-1,4-dicarbonitrile (1.28 g, 10.0 mmol) was dissolved in 20 mL THF, and then under stirring 40 mL of 1 M $LiN(SiMe_3)_2$ solution was added dropwise while cooled with an ice bath (0 ˚C). The obtained mixture was kept at room temperature (25 ˚C) for 3 h, and then cooled back to 0 ˚C. 40 mL of 6 M HCl–EtOH was added to quench the reaction, and the mixture was left overnight before filtration. The precipitate was washed with Et_2O, and the final product (2.26 g, 96%) was recrystallized from H_2O–EtOH mixture. ^1H NMR (400 MHz, DMSO-d6): δ = 9.63 (s, 4H, NH), 9.37 (s, 4H, NH), 8.03 (s, 4H, aromatic H).

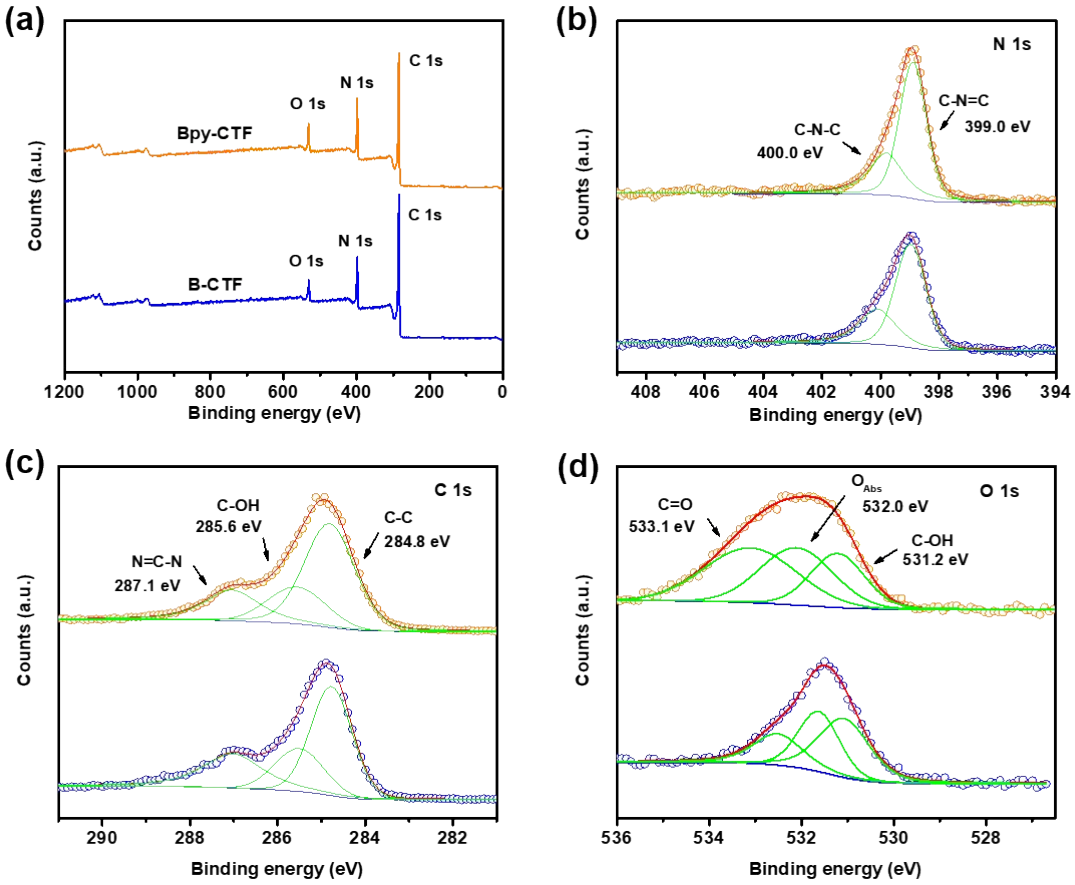

Figure S1. (a) Low-resolution XPS survey. High-resolution XPS spectra of (b) N 1s; (c) C 1s; (d) O 1s of Bpy-CTF (top) and B-CTF (bottom).

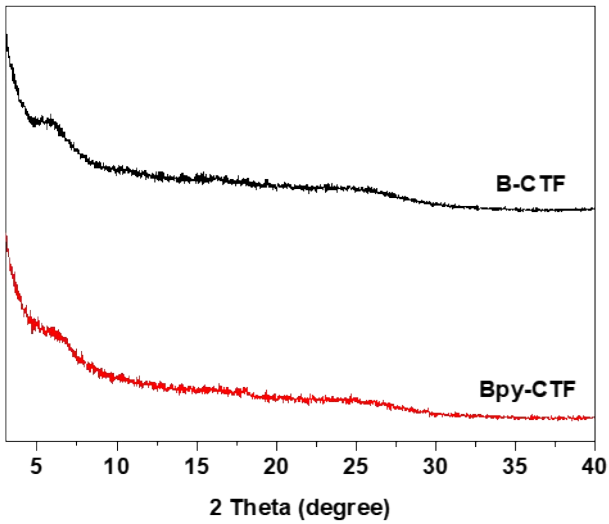

Figure S2. PXRD patterns of Bpy-CTF and B-CTF.

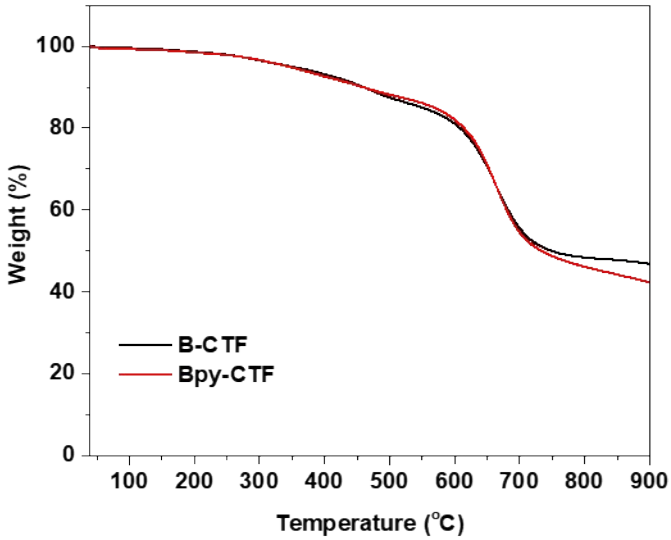

Figure S3. TGA of Bpy-CTF and B-CTF in a nitrogen atmosphere.

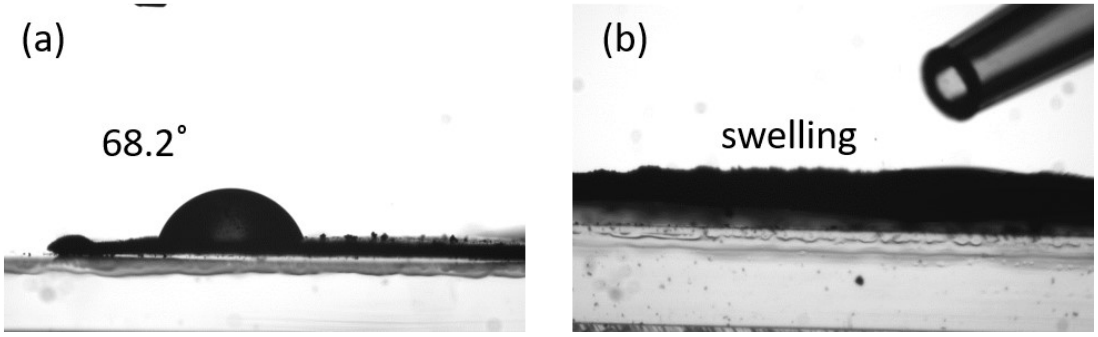

Figure S4. Water contact angles of (a) B-CTF and (b) Bpy-CTF.

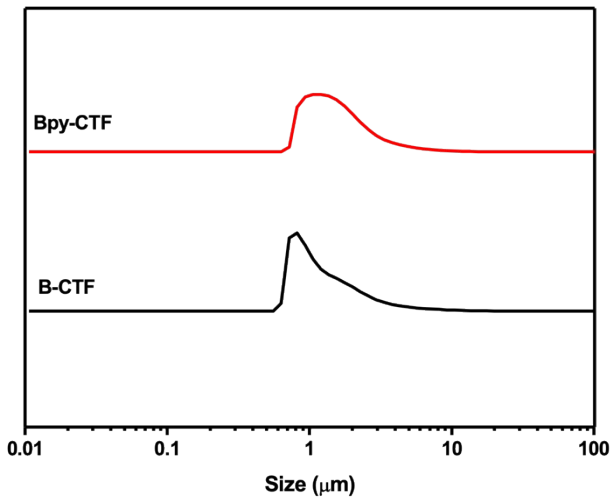

Figure S5. Particle size distribution of (a) Bpy-CTF and (b) B-CTF obtained from static light scattering measurements in water.

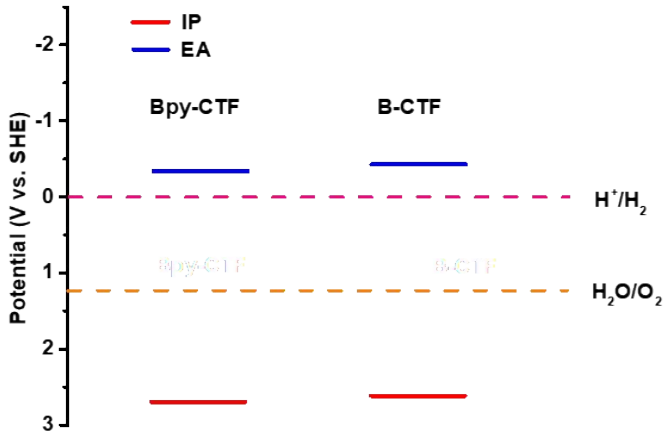

Figure S6. Scheme showing calculated IP, EA of Bpy-CTF and B-CTF [2].

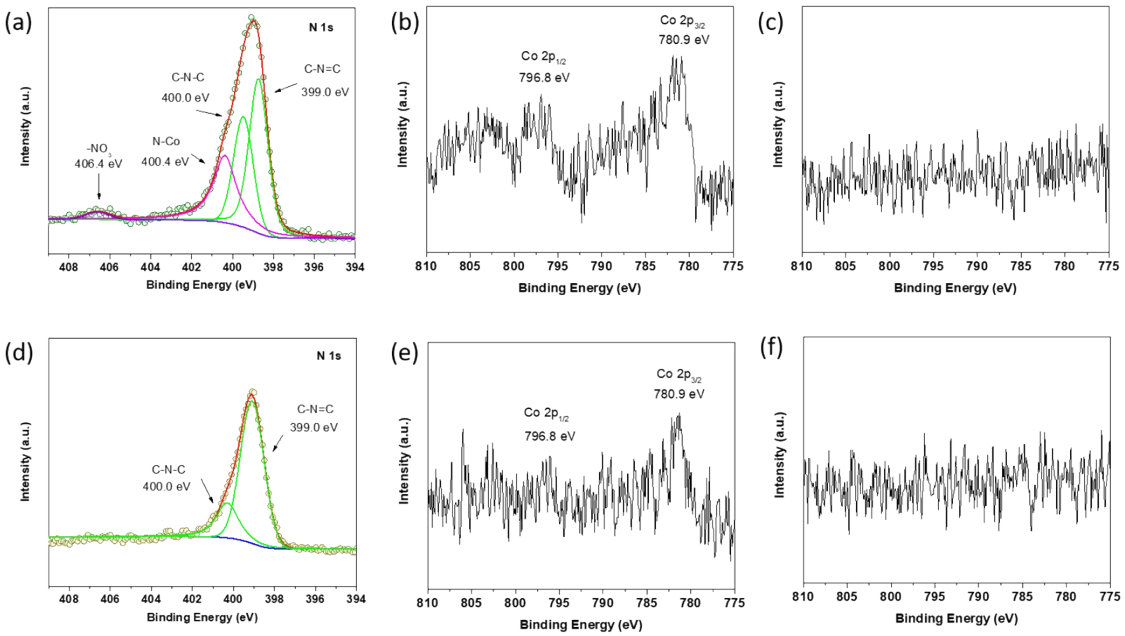

Figure S7. High resolution XPS spectra of (a) N 1s and (b) Co 2p of Bpy-CTF-Co-3; (c) Co 2p of Bpy-CTF; (d) N 1s and (e) Co 2p of B-CTF-Co-3; (f) Co 2p of B-CTF.

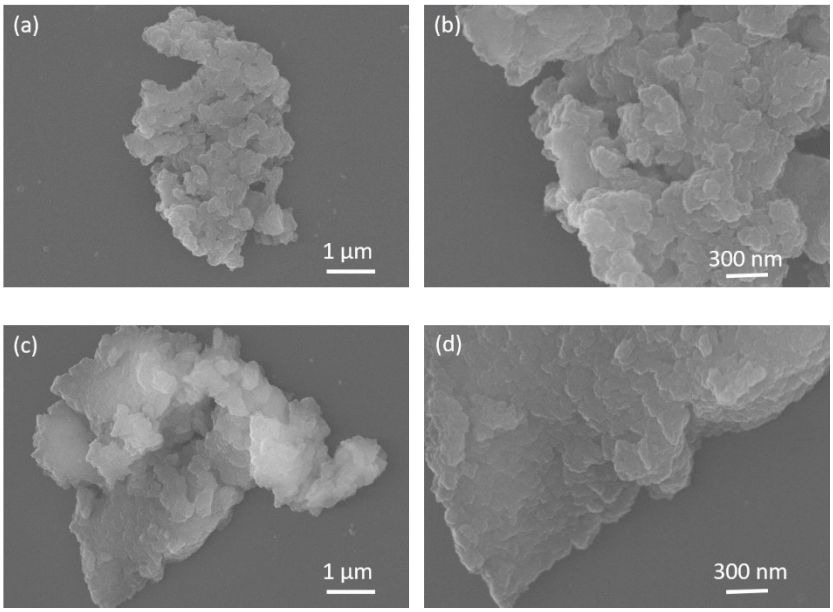

Figure S8. SEM images of (a), (b) Bpy-CTF-Co-1; (c), (d) B-CTF-Co-1.

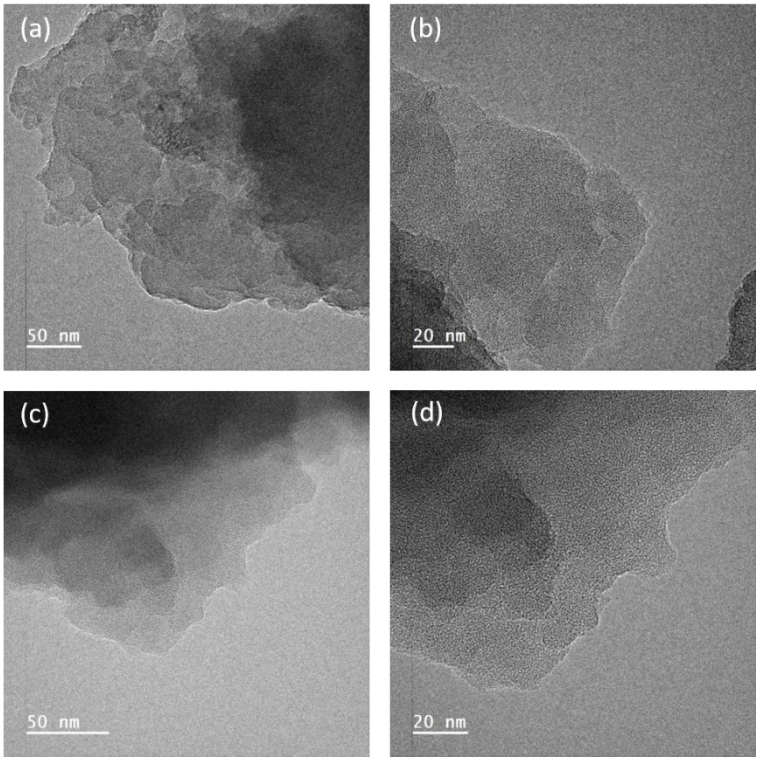

Figure S9. TEM images of (a), (b) Bpy-CTF-Co-1; (c), (d) B-CTF-Co-1.

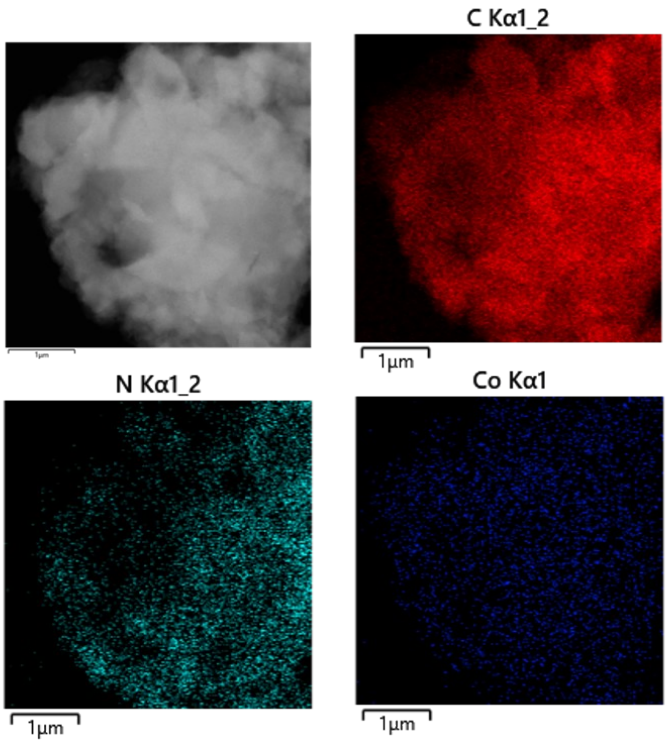

Figure S10. TEM image and element mapping of C, N, and Co of Bpy-CTF-Co-1.

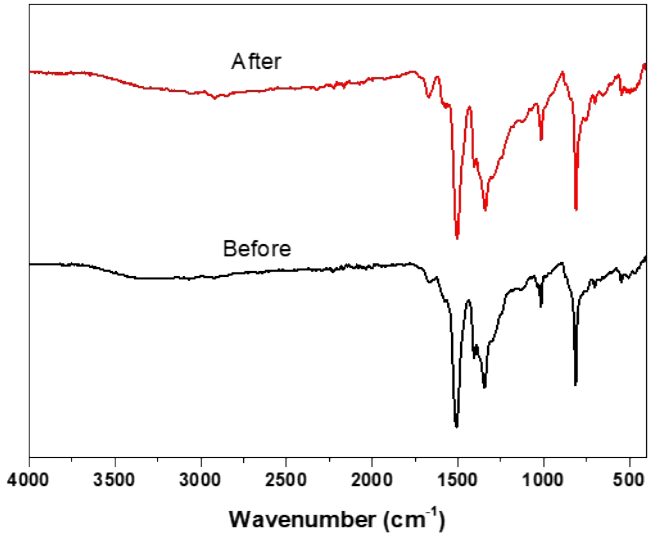

Figure S11. FT-IR spectra of Bpy-CTF-Co-3 before and after oxygen evolution.

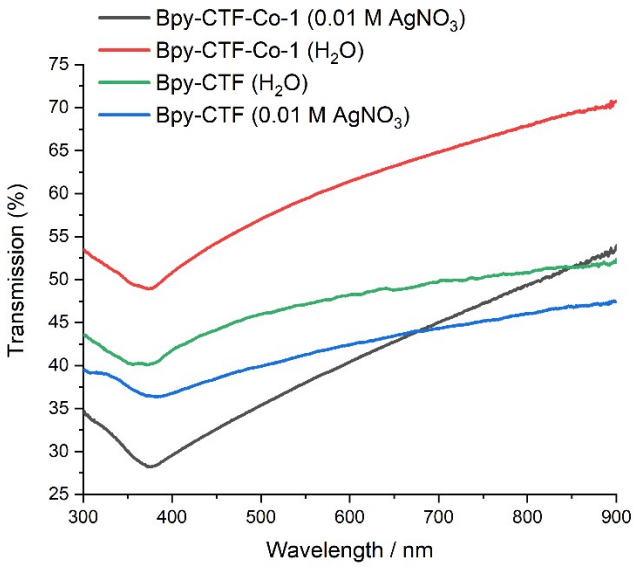

Figure S12. UV/Vis of 2 mg of Bpy-CTF and Bpy-CTF-Co-1 in 20 ml of pure H_2O or 20 ml of 0.01 M $AgNO_3$ in 10 mm pathlength cuvette.

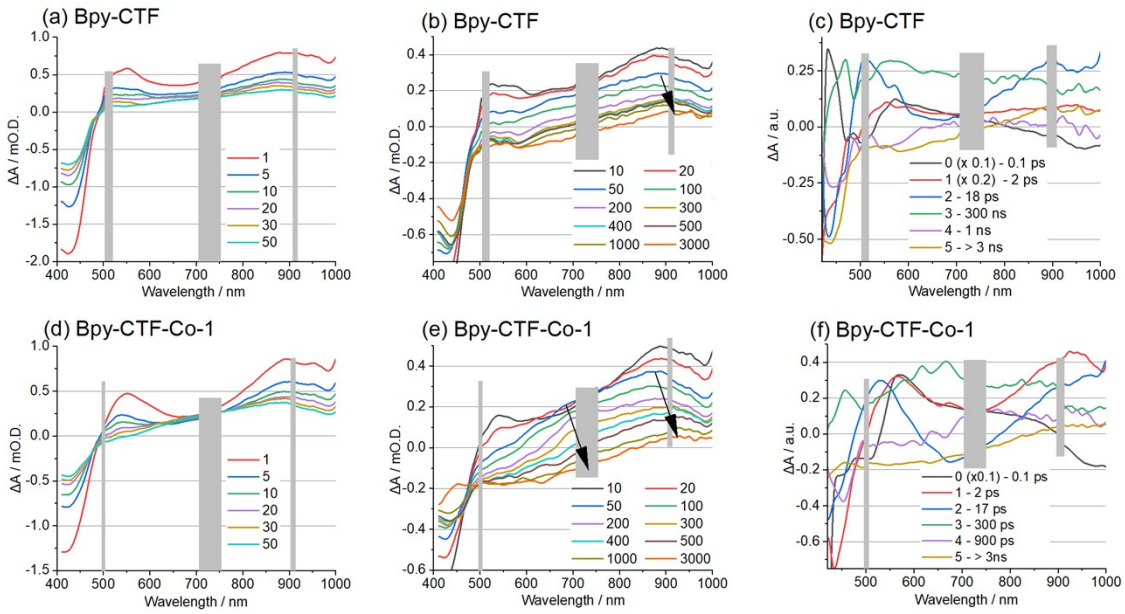

Figure S13. TA spectra (365 nm pump), normalised at the global maximum ΔA, at key pump-probe wavelengths as indicated (in ps) for (a) and (b) Bpy-CTF and (d) and (e) Bpy-CTF-Co-1 in pure H_2O. DADS for (c) Bpy-CTF and (f) Bpy-CTF-Co-1 from a 6-compartment parallel fit; DADS of compartment-0 is scaled by x0.1 for Bpy-CTF and Bpy-CTF-Co-1 and compartment-1 is scaled by x0.2 for Bpy-CTF; decay times for each compartment are indicated. The grey area at ~500 nm and ~900 nm indicates where spectra obtained in different spectral ranges (400 – 500 nm, 500 – 900 nm and 900-1000 nm) have been spliced and between 710 – 755 nm where spectra obtained in a single spectral range (500 – 900 nm) are contaminated by detected pump laser scatter (2λ).

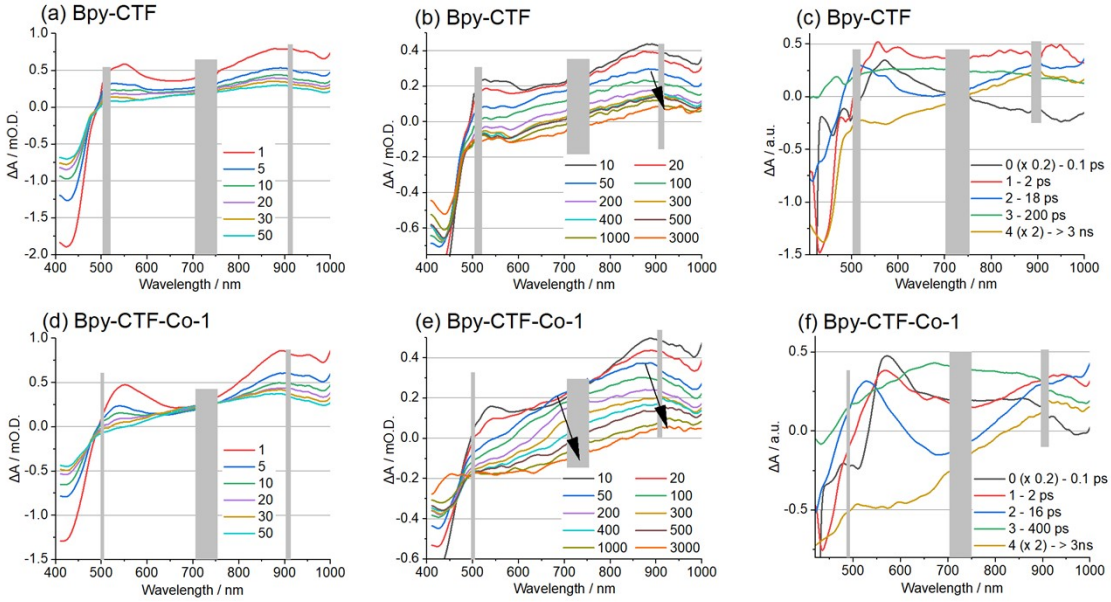

Figure S14. TA spectra (365 nm pump), normalised at the global maximum ΔA, at key pump-probe wavelengths as indicated (in ps) for (a) and (b) Bpy-CTF and (d) and (e) Bpy-CTF-Co-1 in pure H_2O. DADS for (c) Bpy-CTF and (f) Bpy-CTF-Co-1 from a 5-compartment parallel fit; DADS of compartment-0 is scaled by x0.2 and compartment-4 is scaled by x2 for Bpy-CTF and Bpy-CTF-Co-1; decay times for each compartment are indicated. The grey area at ~500 nm and ~900 nm indicates where spectra obtained in different spectral ranges (400 – 500 nm, 500 – 900 nm and 900-1000 nm) have been spliced and between 710 – 755 nm where spectra obtained in a single spectral range (500 – 900 nm) are contaminated by detected pump laser scatter (2λ). **Note the poor agreement between compartment 4 and the 3 ns TA spectrum in the 600 – 700 nm region of Bpy-CTF and in the 400 – 550 and 675 – 800 nm regions for Bpy-CTF-Co-1.**

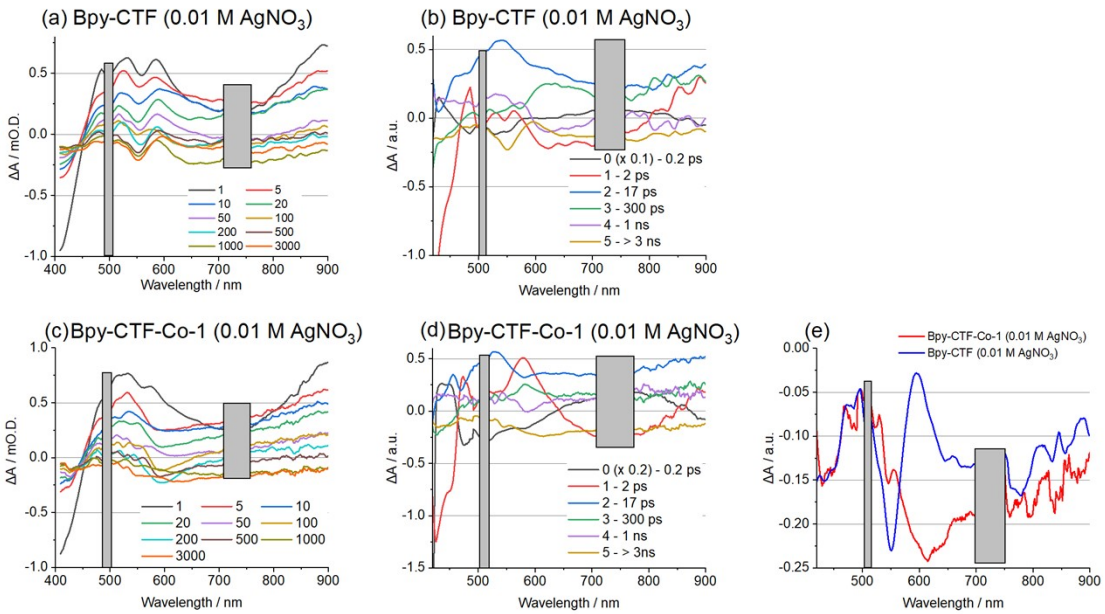

Figure S15. TA spectra (365 nm pump)), normalised at the global maximum ΔA, at key pump-probe wavelengths as indicated (in ps) for (a) Bpy-CTF and (c) Bpy-CTF-Co-1 in 0.01 M $AgNO_3$. DADS for (b) Bpy-CTF and (d) Bpy-CTF-Co-1 from a 6-compartment parallel fit; DADS of compartment-0 is scaled by x0.1 and x0.2 for Bpy-CTF and Bpy-CTF-Co-1 respectively; decay times for each compartment are indicated. (e) Comparison of the DADS of compartment 5 for Bpy-CTF (blue) and Bpy-CTF-Co-1(red). The grey area at ~500 nm indicates where spectra obtained in different spectral ranges (400 – 500 nm and 500 – 900 nm) have been spliced, and between 710 – 755 nm where spectra obtained in a single spectral range (500 – 900 nm) are contaminated by detected pump laser scatter (2λ).

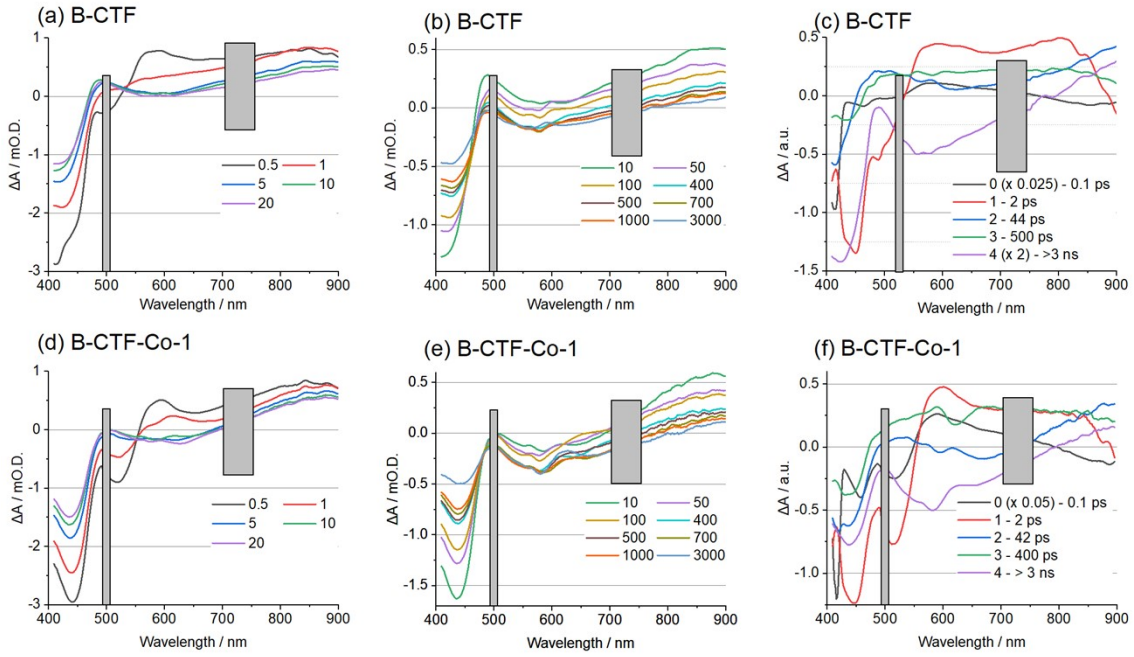

Figure S16. TA spectra (365 nm pump), normalised at the global maximum ΔA, at key pump-probe wavelengths as indicated (in ps) for (a) and (b) B-CTF and (d) and (e) B-CTF-Co-1 in pure H_2O. DADS for (c) B-CTF and (f) B-CTF-Co-1 from a 5-compartment parallel fit; DADS of compartment-0 is scaled by x0.025 and x0.05 for B-CTF and B-CTF-Co-1 respectively, and DADS of compartment 4 scaled by x2 for B-CTF; decay times for each compartment are indicated. The grey area at ~500 nm indicates where spectra obtained in different spectral ranges (400 – 500 nm, 500 – 900 nm and 900-1000 nm) have been spliced and between 710 – 755 nm where spectra obtained in a single spectral range (500 – 900 nm) are contaminated by detected pump laser scatter (2λ).

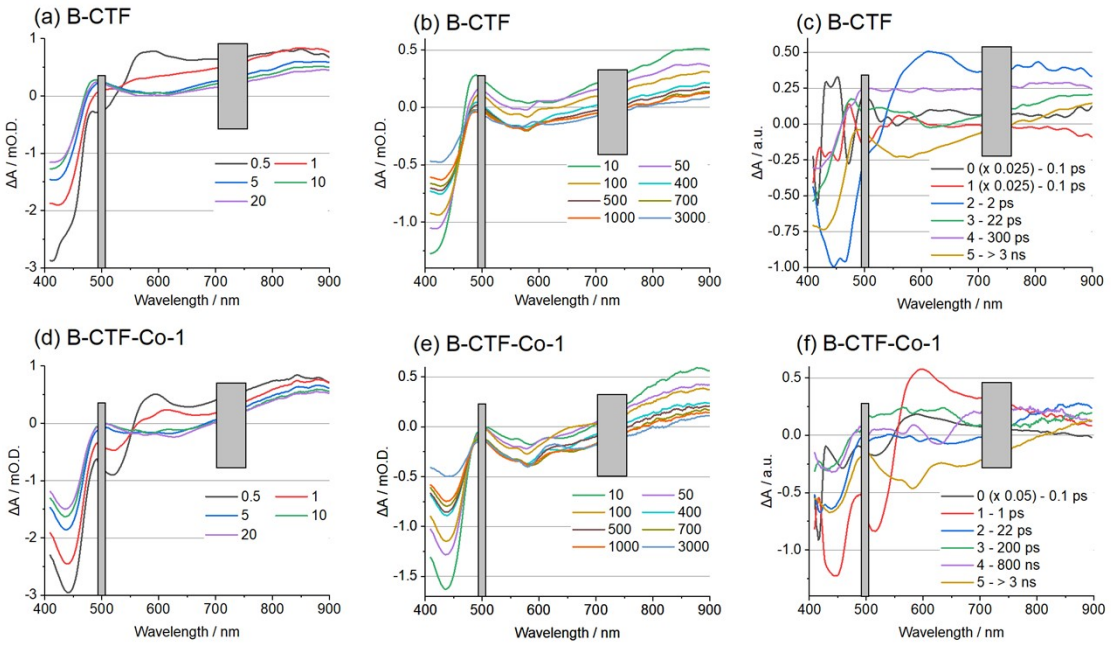

Figure S17. TA spectra (365 nm pump), normalised at the global maximum ΔA, at key pump-probe wavelengths as indicated (in ps) for (a) and (b) B-CTF and (d) and (e) B-CTF-Co-1 in pure H_2O. DADS for (c) B-CTF and (f) B-CTF-Co-1 from a 6-compartment parallel fit; DADS of compartment-0 is scaled by x0.025 and x0.05 for B-CTF and B-CTF-Co-1 respectively, and DADS of compartment-1 scaled by x0.05 for B-CTF; decay times for each compartment are indicated. The grey area at ~500 nm indicates where spectra obtained in different spectral ranges (400 – 500 nm, 500 – 900 nm and 900-1000 nm) have been spliced and between 710 – 755 nm where spectra obtained in a single spectral range (500 – 900 nm) are contaminated by detected pump laser scatter (2λ).

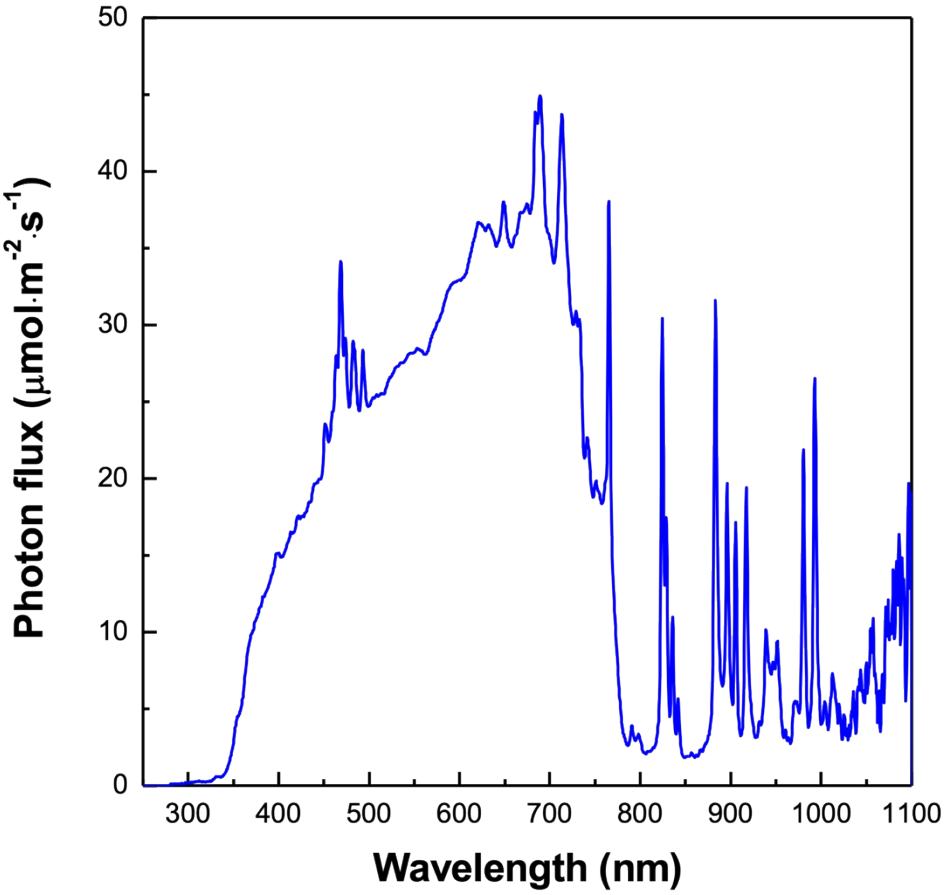

Figure S18. The emission spectrum and the intensity of the 300 W Xenon lamp.

Table S1. Elemental analysis results of Bpy-CTF and B-CTF.

	N (%)		C (%)		H (%)	
	Exp.	Cal.	Exp.	Cal.	Exp.	Cal.
Bpy-CTF	21.41	27.76	65.19	66.65	3.25	5.59
B-CTF	15.55	20.40	69.66	74.98	3.81	46.1

Table S2. Optical gap, band positions and oxygen evolution rates (OERs) of Bpy-CTF and B-CTF.

	Optical gap (eV)	Water contact angle (˚)	Transmittance (%)	OER[a] (μmol g^{-1} h^{-1})
Bpy-CTF	2.21	-[b]	1.95	322
B-CTF	2.07	68.2	1.38	162

[a]Reaction conditions: 10 mg CTF photocatalysts loaded with 3 wt.% cobalt was suspended in water/$AgNO_3$/La_2O_3, 300 W Xe light source visible light (≥ 420 nm) irradiation; [b]Not determined as sample swells in contact with water

Table S3. ICP analysis result of Bpy-CTF-Co-x and B-CTF-Co-x.

	Initial Co loading (wt. %)	Co amount (ICP result) (wt. %)
Bpy-CTF-Co-0.5	0.5	0.48
Bpy-CTF-Co-1	1	0.72
Bpy-CTF-Co-3	3	2.50
Bpy-CTF-Co-5	5	3.66
B-CTF-Co-1	1	0.29
B-CTF-Co-3	3	0.90

Table S4. Estimated fluorescence life-times calculated from time correlated single photon counting measurements results.

CTFs	τ_1[a]	B_1[a]	τ_2[a]	B_2[a]	τ_3[a]	B_3[a]	χ^2	τ_{AVG}[b]
	(ns)	(%)	(ns)	(%)	(ns)	(%)		(ns)
Bpy-CTF	0.563	47.258	2.389	45.892	9.12	6.849	1.219	1.99
Bpy-CTF-Co-3	0.487	65.46	2.222	31.955	10.766	2.585	1.695	1.31

[a]Fluorescence life-times for all polymers in ethanol suspension obtained from fitting time-correlated single photon counting decays to a sum of three exponentials, which yield τ_1, τ_2, and τ_3 according to $\sum_{i=1}^{n}(A + B_i exp(-\frac{t}{\tau_i}))$. [b]$\tau_{AVG}$ is the weighted average lifetime calculated as $\sum_{i=1}^{n} B_i \tau_i$.

Table S5. Overview of reported polymer photocatalysts for OER.

	Band gap (eV)	Co-catalyst	Sacrificial agent	OER ($\mu mol\ g^{-1}\ h^{-1}$)	AQY (%)	Light source	Ref.
Bpy-CTF	2.21	3 wt.% Co	0.01 M $AgNO_3$, 0.2 g La_2O_3	322 (≥ 420 nm)	0.56 (420 nm)	300 W Xe	This work
CTP-2	2.66	3 wt.% Co	0.01 M $AgNO_3$, 0.2 g La_2O_3	100 (> 300 nm) 50 (≥ 420 nm)	-	300 W Xe	[3]
g-C_3N_4	2.76	3 wt.% $Co(OH)_2$	0.01 M $AgNO_3$, 0.2 g La_2O_3	548 (> 300 nm) 142 (> 420 nm)	-	300 W Xe	[4]
CTF-1-100W	2.50	3 wt.% RuO_x	0.2 M $AgNO_3$ (0.05 M $AgNO_3$)	140 (> 420 nm)	3.8 (420 nm)	300 W Xe	[5]
CTF-T1	2.94	RuO_2	0.01 M $AgNO_3$, 0.2 g La_2O_3	9 (> 420 nm)	-	300 W Xe	[6]
P10	2.62	1 wt.% Co	0.01 M $AgNO_3$, 0.2 g La_2O_3	104 (> 420 nm), 332 (full arc)	-	300 W Xe	[7]
BpCo-COF-1	2.41	1 wt.% Co	0.005 M $AgNO_3$	152 (> 420 nm)	0.46 (420 nm)	300 W Xe	[8]
g-$C_{40}N_3$-COF	2.36	3 wt.% Co	0.01 M $AgNO_3$, 0.2 g La_2O_3	50 (> 420 nm)		300 W Xe	[9]
aza-CMP nanosheet	1.22	3 wt.% $Co(OH)_2$	0.01 M $AgNO_3$, La_2O_3	572 (> 420 nm)	-	300 W Xe	[10]
Urea-PDI	1.79	None	0.05 M $AgNO_3$, 0.1 g La_2O_3	3223.9 (> 420 nm)	3.86 (450 nm)	300 W Xe	[11]
PTPP	1.52	None	0.01 M $AgNO_3$, La_2O_3	236 (> 420 nm)	2.11 (420 nm)	300 W Xe	[12]
PQL	1.72	None	0.01 M $AgNO_3$, La_2O_3	60 (> 420 nm)	0.43 (420 nm)	300 W Xe	[12]

References

[1] K. Wang, L.M. Yang, X. Wang, L. Guo, G. Cheng, C. Zhang, S. Jin, B. Tan, A. Cooper, Covalent Triazine Frameworks via a Low-Temperature Polycondensation Approach, Angew. Chemie - Int. Ed. 56 (2017) 14149–14153. https://doi.org/10.1002/anie.201708548.

[2] L. Guo, X. Wang, Z. Zhan, Y. Zhao, L. Chen, T. Liu, B. Tan, S. Jin, Crystallization of Covalent Triazine Frameworks via a Heterogeneous Nucleation Approach for Efficient Photocatalytic Applications, Chem. Mater. 33 (2021) 1994–2003. https://doi.org/10.1021/acs.chemmater.0c03716.

[3] Z.A. Lan, Y. Fang, Y. Zhang, X. Wang, Photocatalytic Oxygen Evolution from Functional Triazine-Based Polymers with Tunable Band Structures, Angew. Chemie - Int. Ed. 57 (2018) 470–474. https://doi.org/10.1002/anie.201711155.

[4] G. Zhang, S. Zang, X. Wang, Layered Co(OH)2 deposited polymeric carbon nitrides for photocatalytic water oxidation, ACS Catal. 9 (2015) 941–947. https://doi.org/10.1021/cs502002u.

[5] J. Xie, S.A. Shevlin, Q. Ruan, S.J.A. Moniz, Y. Liu, X. Liu, Y. Li, C.C. Lau, Z.X. Guo, J. Tang, Efficient visible light-driven water oxidation and proton reduction by an ordered covalent triazine-based framework, Energy Environ. Sci. 11 (2018) 1617–1624. https://doi.org/10.1039/c7ee02981k.

[6] J. Bi, W. Fang, L. Li, J. Wang, S. Liang, Y. He, M. Liu, L. Wu, Covalent Triazine-Based Frameworks as Visible Light Photocatalysts for the Splitting of Water, Macromol. Rapid Commun. 36 (2015) 1799–1805. https://doi.org/10.1002/marc.201500270.

[7] R.S. Sprick, Z. Chen, A.J. Cowan, Y. Bai, C.M. Aitchison, Y. Fang, M.A. Zwijnenburg, A.I. Cooper, X. Wang, Water oxidation with cobalt-loaded linear conjugated polymer photocatalysts, Angew. Chemie Int. Ed. 132 (2020) 18854–18859. https://doi.org/10.1002/anie.202008000.

[8] J. Chen, X. Tao, C. Li, Y. Ma, L. Tao, D. Zheng, J. Zhu, H. Li, R. Li, Q. Yang, Synthesis of bipyridine-based covalent organic frameworks for visible-light-driven photocatalytic water oxidation, Appl. Catal. B Environ. 262 (2020) 1–8. https://doi.org/10.1016/j.apcatb.2019.118271.

[9] S. Bi, C. Yang, W. Zhang, J. Xu, L. Liu, D. Wu, X. Wang, Y. Han, Q. Liang, F. Zhang, Two-dimensional semiconducting covalent organic frameworks via condensation at arylmethyl carbon atoms, Nat. Commun. 10 (2019) 1–10. https://doi.org/10.1038/s41467-019-10504-6.

[10] L. Wang, Y. Wan, Y. Ding, Y. Niu, Y. Xiong, X. Wu, H. Xu, Photocatalytic oxygen evolution from low-bandgap conjugated microporous polymer nanosheets: a combined first-principles calculation and experimental study, Nanoscale. 9 (2017) 4090–4096. https://doi.org/10.1039/c7nr00534b.

[11] Z. Zhang, X. Chen, H. Zhang, W. Liu, W. Zhu, Y. Zhu, A Highly Crystalline Perylene Imide Polymer with the Robust Built-In Electric Field for Efficient Photocatalytic Water Oxidation, Adv. Mater. 1907746 (2020) 1–6. https://doi.org/10.1002/adma.201907746.

[12] X. Ma, H. Wang, J. Cheng, H. Cheng, L. Wang, X. Wu, H. Xu, Fully Conjugated Ladder Polymers as Metal-Free Photocatalysts for Visible-Light-Driven Water Oxidation, Chinese J. Chem. 39 (2021) 1079–1084. https://doi.org/10.1002/cjoc.202000614.